# Roll-to-Roll Printed Silver Nanowire Semitransparent Electrodes for Fully Ambient Solution-Processed Tandem Polymer Solar Cells

*Dechan Angmo, Thomas R. Andersen, Janet J. Bentzen, Martin Helgesen, Roar R. Søndergaard, Mikkel Jørgensen, Jon E. Carlé, Eva Bundgaard, and Frederik C. Krebs**

**Silver nanowires (AgNWs) and zinc oxide (ZnO) are deposited on flexible substrates using fast roll-to-roll (R2R) processing. The AgNW film on polyethylene terephthalate (PET) shows >80% uniform optical transmission in the range of 550–900 nm. This electrode is compared to the previously reported and currently widely produced indium-tin-oxide (ITO) replacement comprising polyethylene terephthalate (PET)|silver grid|poly(3,4-ethylenedioxythiophene):poly(styrenesulfonate) (PEDOT:PSS)|ZnO known as Flextrode. The AgNW/ZnO electrode shows higher transmission than Flextrode above 490 nm in the electromagnetic spectrum reaching up to 40% increased transmission at 750 nm in comparison to Flextrode. The functionality of AgNW electrodes is demonstrated in single and tandem polymer solar cells and compared with parallel devices on traditional Flextrode. All layers, apart from the semitransparent electrodes which are large-scale R2R produced, are fabricated in ambient conditions on a laboratory roll-coater using printing and coating methods which are directly transferrable to large-scale R2R processing upon availability of materials. In a single cell structure, Flextrode is preferable with active layers based on poly-3-hexylthiophene(P3HT):phenyl-C61-butyric acid methylester (PCBM) and donor polymers of similar absorption characteristics while AgNW/ZnO electrodes are more compatible with low band gap polymer-based single cells. In tandem devices, AgNW/ZnO is more preferable resulting in up to 80% improvement in PCE compared to parallel devices on Flextrode.**

## 1. Introduction

The evolving nature of optoelectronic applications imposes new demands on prospective indium-tin-oxide (ITO) replacements with flexibility, low cost, and compatibility with large-scale and fast manufacturing methods deemed as crucial criteria. ITO is the commonly employed transparent conductor in optoelectronic applications in general and polymer solar cells (PSCs) in particular. However, ITO is expensive, brittle, requires multistep processing, and it is estimated to ultimately account for 90% of the total embedded energy in a PSC module.[1,2] The inherent limitation of the stability of PSCs cast rigorous cost restrictions in the choice of materials and processing methods which have to be highly simplified despite the increasing efficiency that has reached values close to some inorganic photovoltaic technologies.[3,4] Hence, studies on replacement of ITO have been rather intensive in the past few years.

Silver nanowires represent a very favorable proposition for PSCs.[5–8] Random networks of silver nanowires (AgNWs) can display transmission and sheet resistance similar, or even superior to ITO. AgNWs are synthesized via a wet chemical route[8] at low temperatures and can be dispersed in a range of solvents in very low concentration which in turn is suitable for further deposition on a substrate using a range of coating and printing methods. Solution-processing techniques such as spray-coating,[9–12] drop-casting,[13–15] spin-coating,[16–18] doctor-blading,[17] rod-coating,[19–21] have so far been demonstrated. Finally, random networks of AgNWs on flexible substrates display much greater flexibility than ITO.[21,22] Several reviews and articles on AgNWs have been reported.[6,8]

Despite many advantages, the use of silver nanowires in PSCs has faced several challenges. Inarguably, the biggest challenge is the rough topology of AgNWs films which leads to penetration of the protruding wires through the active layer to the counter electrode, thus causing short circuits in the devices. Glancing through the literature, the situation seems worse when a flexible substrate is employed.[23,24] To overcome this, several methods have been explored including the use of optical sintering,[25] electrical annealing,[26] subjection to mechanical compression at high pressure,[24] and processing strategies including the use of very thick active layers,[27] thick buffer layers such as metal oxides and PEDOT:PSS,[17] a transfer-based

Dr. D. Angmo, Dr. T. R. Andersen, J. J. Bentzen, Dr. M. Helgesen, Dr. R. R. Søndergaard, Dr. M. Jørgensen, Dr. J. E. Carlé, Dr. Eva Bundgaard, Prof. F. C. Krebs
Department of Energy Conversion and Storage
Technical University of Denmark
Frederiksborgvej 399, 4000 Roskilde, Denmark
E-mail: frkr@dtu.dk

**DOI: 10.1002/adfm.201501887**

method,[28,29] to name a few. While these techniques may appear feasible with small area devices as they are generally demonstrated on areas less than 0.1 $cm^2$; however, several of these methods cannot be transferred to a fast processing method and realized on larger areas without adding to cost and/or loss of efficiency.

Recently, we have demonstrated a multistack electrode known as Flextrode as an ITO alternative.[30–33] Flextrode comprises of polyethylene terephthalate (PET)/Ag grid/PEDOT:PSS/zinc oxide (ZnO) manufactured through a robust high speed roll-to-roll (R2R) processing using printing and coating steps under ambient conditions. This electrode is optimal for poly-3-hexylthiophene (P3HT):phenyl-C61-butyric acid methylester (PCBM) as its peak transmission region coincides with the absorption region of P3HT:PCBM and polymers of similar optical absorption characteristics. However, the transmission of Flextrode is significantly lower at longer wavelengths of the electromagnetic spectrum due to the use of PEDOT:PSS that absorbs in the near infrared, thus making it unsuitable for single cells based on low band gap polymers and tandem solar cells that employ low band gap polymers. These limitations were explored and realized in a recent study on large-scale roll-to-roll processing of flexible PSC tandem modules.[34] This limitation led us to develop AgNW films through a robust process that is suitable for large area fabrication.[35] Although the literature is filled with reports of high efficiency PSCs with AgNW substrate electrodes, the investigated area is generally very small. Such studies and the processing techniques reported therein do not justify their applicability on a large scale, particularly when AgNWs present the challenge of creating short circuits which increasingly manifests itself as the active area increases.

In this paper, we demonstrate the fabrication of single and tandem junctions on AgNW network films through roll-to-roll based large-scale processing using rotary screen printing (RSP) and explore the advantages that AgNW based electrodes potentially have to offer over traditional Flextrode. With the addition of a superseding ZnO layer, we are able to achieve a robust electrode that can be applied in single junction and tandem PSCs. The electrode is thoroughly characterized and is employed in the roll-to-roll compatible processing of PSCs in single and tandem structures using a directly up-scalable design and an area of ≈1 $cm^2$. The AgNW/ZnO electrode is compared to Flextrode and both single junction and tandem devices built on AgNW/ZnO are compared to devices on traditional Flextrode.

## 2. Results and Discussion

### 2.1. AgNW and Flextrode as Transparent Electrode

A comparison of the front electrodes for PSC modules prepared with Flextrode and AgNW film on PET is shown in **Figure 1**. Both samples are completely solution processed using the same roll-to-roll line. Both samples are processed in stripes of 1 cm width along the length of the PET substrate and the design shown in Figure 1 is a standard design which we employ in the fabrication of serially connected large area modules.[30,32] In this paper, we employ such substrates to fabricate single cells along each stripe as described in detail later on.

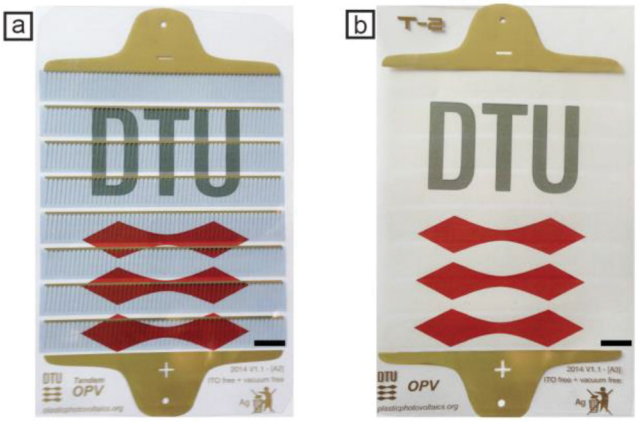


**Figure 1.** Roll-to-roll processed ITO-free transparent electrodes are shown: a) Flextrode and b) AgNW/ZnO. Scale bar is 1 cm.

The contribution of this paper to the progress of AgNWs as transparent electrode is that we have fabricated AgNWs in a roll-to-roll process using only one-step RSP resulting in a good network of AgNWs (**Figure 2**). Details on the RSP process can be found elsewhere.[36,37] By changing the concentration, we can optimize the transmission and sheet resistance. Using a commercial ink, the AgNW film displays >80% transmittance in the visible region with a sheet resistance of 10–20 Ω $\square^{-1}$. Figure 2 shows the scanning electron microscopy (SEM) images of roll-to-roll RSP AgNWs revealing that AgNWs have formed a good network which remains consistent over larger areas. Due to the high aspect ratio and nanoscale diameters which means higher surface-to-bulk ratio, AgNW tends to degrade rapidly in ambient conditions due to oxidation.[21,38,39] The application of ZnO or other metal oxides on top of AgNW provides a barrier, thus significantly reducing the rate of oxidation of the AgNW.[38,39] ZnO is also applied on the AgNW film through RSP immediately after the printing of AgNWs. The processing of AgNW and ZnO requires only a short drying time which allows for high web speed roll-to-roll printing. We applied a web speed of 10–20 m $min^{-1}$ with a drying time of less than half a minute at 140 °C and processed them in stripes as shown in Figure 1.

Due to the high aspect ratio of AgNWs, short circuits (shunting) have been the main challenge with the use of AgNWs[29] in PSCs due to interelectrode penetration of AgNWs as described in the Introduction. We observed that the use of 40 nm thick RSP ZnO film results in complete coverage of the AgNW film and no protruding AgNWs out-of-the-plane off the superseding ZnO film were observed (Figure 2). The rotary screen printing process in which the movement of the squeegee induces shear forces on the AgNW ink may have aided in leveling the nanowires flat on the surface of the substrate.

Scattering makes a significant contribution to transmission of AgNWs which effectively contributes to the charge generation in PSCs. Therefore, we measured the optical transmission using an integrating sphere that takes into account scattered and direct transmission (**Figure 3**). With the optimized conditions, AgNWs film showed a resistance of 10–20 Ω $\square^{-1}$ with a corresponding total transmission of ≈84% which remains uniform in the range of 550–800 nm. The application of a ZnO

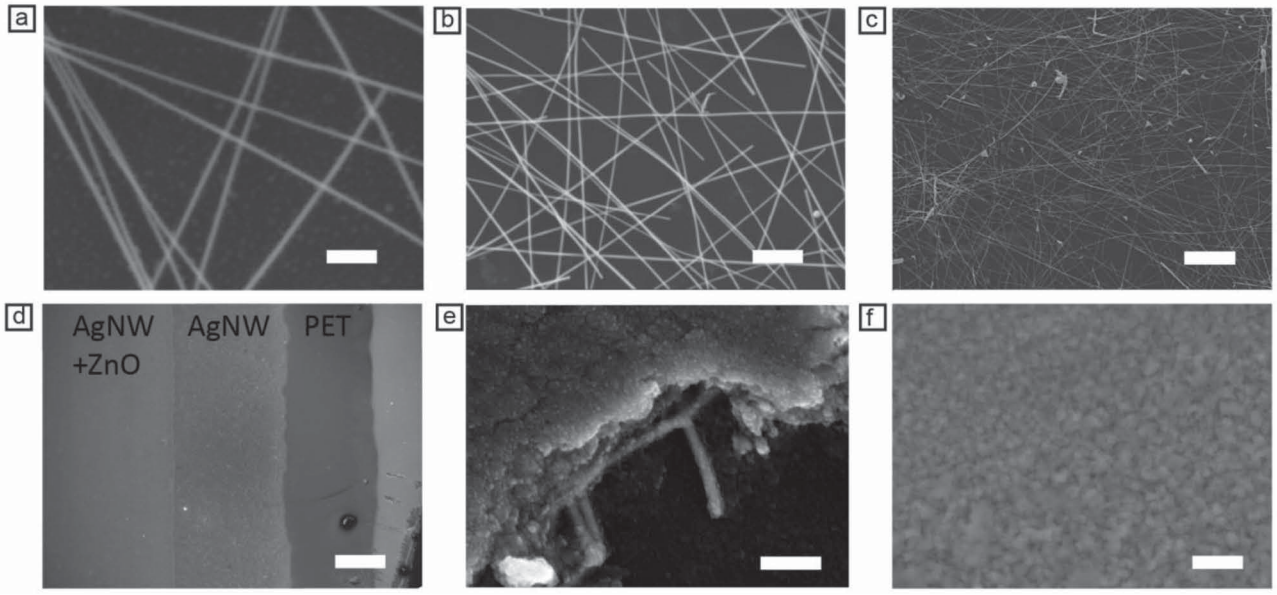


**Figure 2.** SEM images of rotary screen printed AgNW on PET is shown on three different scales. The scale bars correspond to a) 250 nm, b) 500 nm, and c) 5 µm, respectively. The edge of roll-to-roll RSP layers are shown in (d). A close-up is given in (e) that shows AgNW neatly embedded under the ZnO layer. The surface of rotary screen printed ZnO in the middle of printed width is shown in (f) with no visible wire protrusion from the underlying AgNW film. Scale bar in (d–f) corresponds to 200 µm, 200 nm, and 500 nm, respectively.

layer over the AgNWs diminishes the transmission below 550 nm and the AgNW/ZnO film displayed a different characteristic UV cut-off from either pure ZnO or AgNW film as observed in other studies as well.[39] The AgNW/ZnO was stored in a box with nitrogen flow and was employed in fabricating single and tandem cells for this study over a course of 4–5 months. The transmission and sheet resistance of the AgNW stabilized after an initial degradation. Figure 3 presents a comparison between the transmission of the stored AgNW/ZnO film and a freshly fabricated AgNW film. The stored sample showed <10% decline in transmission with a corresponding sheet resistance increase to 30 Ω □$^{-1}$.

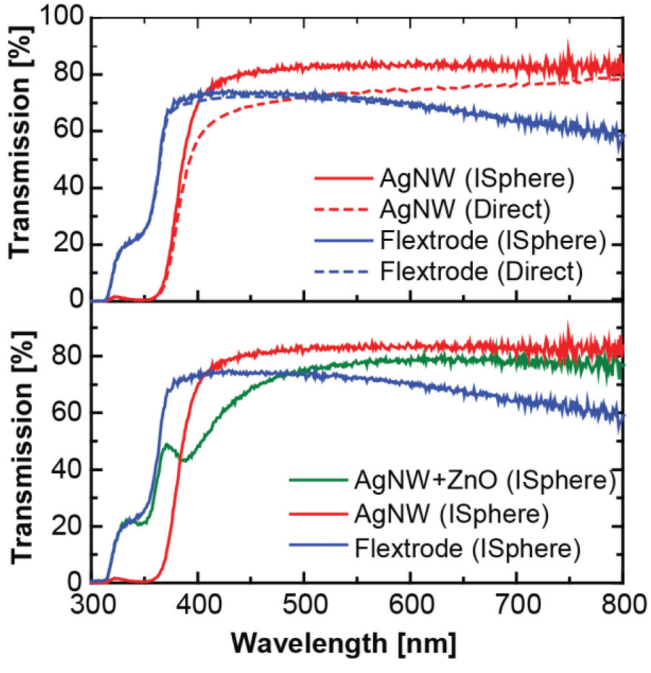


**Figure 3.** Transmission profiles of Flextrode and silver nanowire electrodes (top). ISphere indicates measurement with integrated sphere that takes into account scattered and direct transmission. The evolution of transmission in the stored AgNW/ZnO sample (green line) over four months (bottom). The reference is air.

### 2.2. Polymer Solar Cells

Polymer solar cells in single and tandem architecture were fabricated in an all-solution based process. 1 m long pieces cut from the roll-to-roll fabricated AgNW/ZnO substrate were used to fabricate solar cells on a laboratory roll coater under ambient conditions similar to the processes described elsewhere.[34–42] Parallel devices were fabricated on Flextrode for comparison. The schematic illustrations of tandem devices on Flextrode and AgNWs/ZnO are shown in **Figure 4**. In the single cell structure, the recombination layer and the rear cell as shown in Figure 4 are simply omitted. The polymers used in this study along with their band gaps are listed in **Table 1** and their absorption characteristics are shown in **Figure 5**. The band gaps are calculated from the optical absorption spectra of slot-die coated films on PET and were chosen from our available pool with the intention of fabricating tandem solar cells. The front cells were varied between three polymers PBDTTTz-4:PCBM, P3HT:PCBM, and Polymer Generation 2.1:PCBM while Polymer Generation 2.2:PCBM (the lowest band gap among the pool) was employed as the rear cell in all cases. Although the optical band gap ranges from 1.49 to 1.91 eV covering a broad region of the electromagnetic spectrum, all of the polymers display some overlap between the absorption spectra.

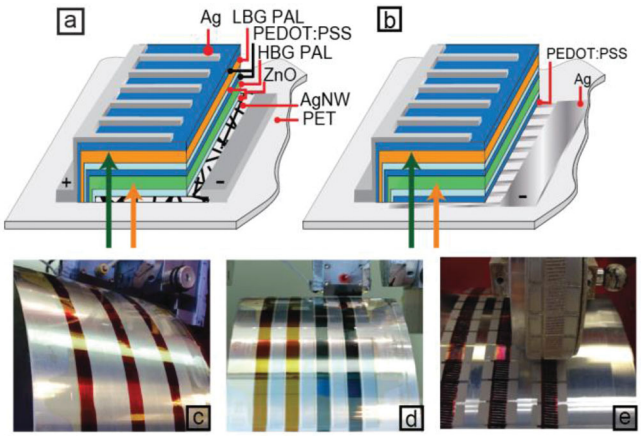


**Figure 4.** Schematic illustration of tandem solar cells on a) AgNW electrode and on b) Flextrode. LBG refers to low band-gap polymer based photoactive layer (PAL) while HBG refers to high band-gap PAL. The R2R coated AgNW/ZnO and Flextrode are used to fabricate solar cells on a roll coater as shown in (c) and (d), respectively. Slot-die coating as shown in (c) and (d) was used in the processing of all layers except for the e) top Ag grid which was flexo printed.

In **Table 2**, the key *IV* parameters are listed for reference single cells with all four polymers while **Figure 6** shows the *IV* curves of the best devices. The Flextrode substrate is more suitable for P3HT:PCBM and PBDTTTz-4:PCBM polymers that generate higher short-circuit current ($J_{sc}$) and fill factor (FF) in comparison to the corresponding devices on AgNW/ZnO. On the other hand, the AgNW substrates are more suitable for lower band gap polymers resulting in higher FF and improved $J_{sc}$ than with the use of Flextrode. On the whole, this trend appears in accordance with the transmission differences of the transparent electrodes with Flextrode having higher transmission in the absorption region of P3HT and PBDTTTz-4 polymers while AgNW/ZnO having higher transmission in the absorption range of low band gap polymers.

The external quantum efficiency (EQE) graphs of all four types of single cells studied here are also shown in Figure 6. All devices on AgNW/ZnO result in improved current generation in the peak absorption region of all the polymers. Integrating the EQE graphs reveal $J_{sc}$ of single cells based on P3HT:PCBM, PBDTTTz-4:PCBM, Polymer Generation 2.1:PCBM, and Polymer Generation 2.2:PCBM to be 5.93, 6.33, 6.24, and 11.33 mA cm$^{-2}$, respectively, on AgNW/ZnO electrode and 6.20, 6.40, 5.42, and 8.46 mA cm$^{-2}$, respectively, on Flextrode. The difference in the $J_{sc}$ values between Flextrode and AgNW/ZnO-based devices for each polymer type is therefore reasonably consistent with the transmission differences of the transparent electrodes.

**Table 1.** List of polymer investigated in this study along with the band gap.

| Polymer | Provider | Optical band gap [eV] |
|---|---|---|
| P3HT | BASF | 1.91 |
| PBDTTTz-4 | In-house[38] | 1.94 |
| Polymer Generation 2.1 | Merck[45] | 1.78 |
| Polymer Generation 2.2 | Merck[45] | 1.49 |

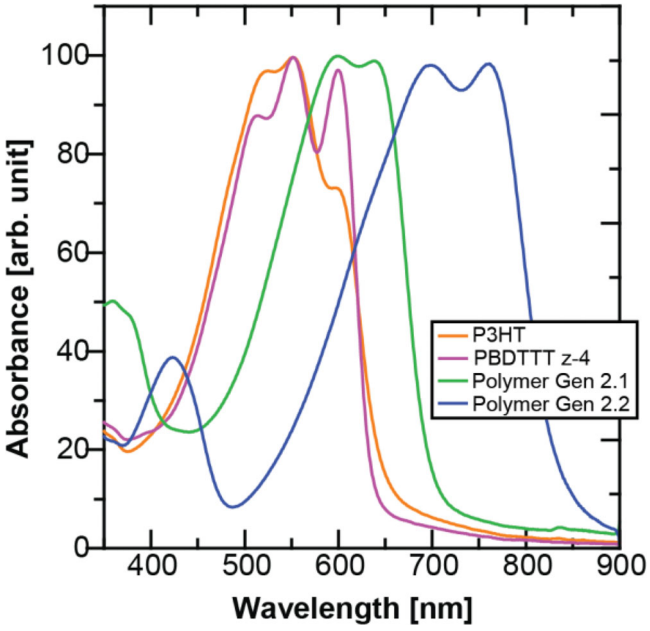


**Figure 5.** Absorption characteristics of the four polymers investigated in this study.

On the other hand, the $J_{sc}$ values of EQE measurement vary greatly from the values measured under simulated AM1.5G conditions provided by a metal–halide lamp (Table 2). Analysis of the spectrum of the solar simulator reveals a large mismatch in the spectrum of the solar simulator and the AM1.5G spectrum (**Figure 7**). The spectrum of the solar simulator is biased toward P3HT and PBDTTTz-4 and against Polymer Generation 2.2 while it is the most accurate for Polymer Generation 2.1 absorption characteristic. The mismatch factor between the spectrum of the solar simulator and the AM1.5 spectrum with respect to the absorption characteristics are calculated for all four polymers (**Table 3**). The mismatch corrected $J_{sc}$ values are also given in the table.

The mismatch corrected $J_{sc}$ of all but Polymer Generation 2.2 fall very close to the EQE values albeit being slightly higher which indicates the presence of an internal field which is overcome under the bias conditions for these three polymers. PBDTTTz-4 shows a 13% increase in $J_{sc}$ value under 1 sun measurement indicating the presence of the strongest field among the three polymers.

On the other hand, while all devices see a slight improvement in $J_{sc}$ under bias conditions irrespective of the type of transparent electrode, only Polymer Generation 2.2:PCBM experiences a drop in $J_{sc}$ under bias conditions in comparison to measured EQE value. Particularly, the $J_{sc}$ of Polymer Generation 2.2:PCBM on AgNW/ZnO is 33% lower than the corresponding measured EQE value. We infer that this is due to very high (monomolecular) nongeminate recombination mechanism being at play in Polymer Generation 2.2 which could be related to poor morphology formation or a poor interface between the active layer and the transparent AgNW/ZnO electrode.[43] The inherently lower FF in comparison to other polymers is the first hand indication of this. The rate of nongeminate recombination depends on charge density,

**Table 2.** *IV* parameters of the best devices and average (minimum four devices) performance of roll-coated single cells on roll-to-roll processed AgNW/ZnO electrode and parallel devices on Flextrode. All measurements are under 1000 W $m^{-2}$ AM1.5G. Areas of all devices are accurately determined using LBIC imaging and are ≈0.8–1 $cm^2$.

| | Flextrode | | | | AgNW | | | |
|---|---|---|---|---|---|---|---|---|
| Polymer | $V_{oc}$ [V] | $J_{sc}$ [mA $cm^{-2}$] | FF [%] | PCE [%] | $V_{oc}$ [V] | $J_{sc}$ [mA $cm^{-2}$] | FF [%] | PCE [%] |
| P3HT (400 nm) | 0.54 (0.54 ± 0.00) | 7.59 (7.02 ± 0.41) | 53.08 (50.72 ± 1.64) | 1.93 (1.72 ± 0.17) | 0.56 (0.56 ± 0.00) | 7.31 (7.76 ± 0.62) | 58.62 (51.02 ± 6.75) | 2.40 (2.20 ± 0.13) |
| PBDTTT (400 nm) | 0.81 (0.81 ± 0.00) | 8.28 (8.35 ± 0.08) | 56.26 (54.82 ± 1.28) | 3.77 (3.71 ± 0.06) | 0.82 (0.81 ± 0.01) | 8.22 (7.75 ± 0.39) | 48.76 (49.13 ± 0.85) | 3.30 (3.09 ± 0.15) |
| Polymer Generation 2.1 (400 nm) | 0.77 (0.77 ± 0.00) | 6.72 (6.14 ± 0.34) | 49.27 (48.55 ± 0.86) | 2.56 (2.29 ± 0.16) | 0.76 (0.76 ± 00) | 7.06 (6.69 ± 0.53) | 51.70 (51.65 ± 3.52) | 2.77 (2.61 ± 0.12) |
| Polymer Generation 2.2 (400) | 0.55 (0.54 ± 0.03) | 6.83 (6.98 ± 0.82) | 33.17 (33.17 ± 1.69) | 1.30 (1.23 ± 0.07) | 0.55 (0.55 ± 00) | 7.16 (7.00 ± 0.16) | 35.22 (34.67 ± 0.48) | 1.38 (1.34 ± 0.04) |

with increasing nongeminate recombination occurring due to higher light intensity, lower carrier mobilities, or lower internal field or a combination thereof.[44] This explains why Polymer Generation 2.2 based on AgNW electrodes shows a $J_{sc}$ value of 11.22 mA $cm^{-2}$ with EQE measurement while it drops by 33% under bias light to 8.09 mA $cm^{-2}$. In comparison, Flextrode-based single cells do not exhibit such a huge difference in EQE measured $J_{sc}$ and *IV*-measured $J_{sc}$ values because of lower charge density generated in comparison to AgNW-based devices owing to the limited transmission of Flextrode in the absorption region of Polymer Generation 2.2. Further investigation into this is beyond the scope of this paper. It may be noted however that Polymer Generation 2.2:PCBM in tandem devices form the rear cell that is coated on top of the same recombination layer in all devices, therefore the interfaces should remain the same in both Flextrode and AgNW-based tandem devices.

**Table 4** shows the *IV* parameters for tandem cells with three different front cells based on P3HT:PCBM, PBDTTTz-4:PCBM, and Polymer Generation 2.1:PCBM and the same rear cell comprising Polymer Generation 2.2:PCBM. The devices are not optimized and universally employ a 250 nm thick front cell and 350 nm thick rear cell. The *IV* curves of the best tandem devices on both types of electrodes are shown in **Figure 8**. All tandem devices on AgNW/ZnO show higher efficiency than the corresponding devices on Flextrode. This is because the rear cell is more efficient in devices based on AgNW/ZnO than on Flextrode despite the mismatch for Polymer Generation 2.2 optical

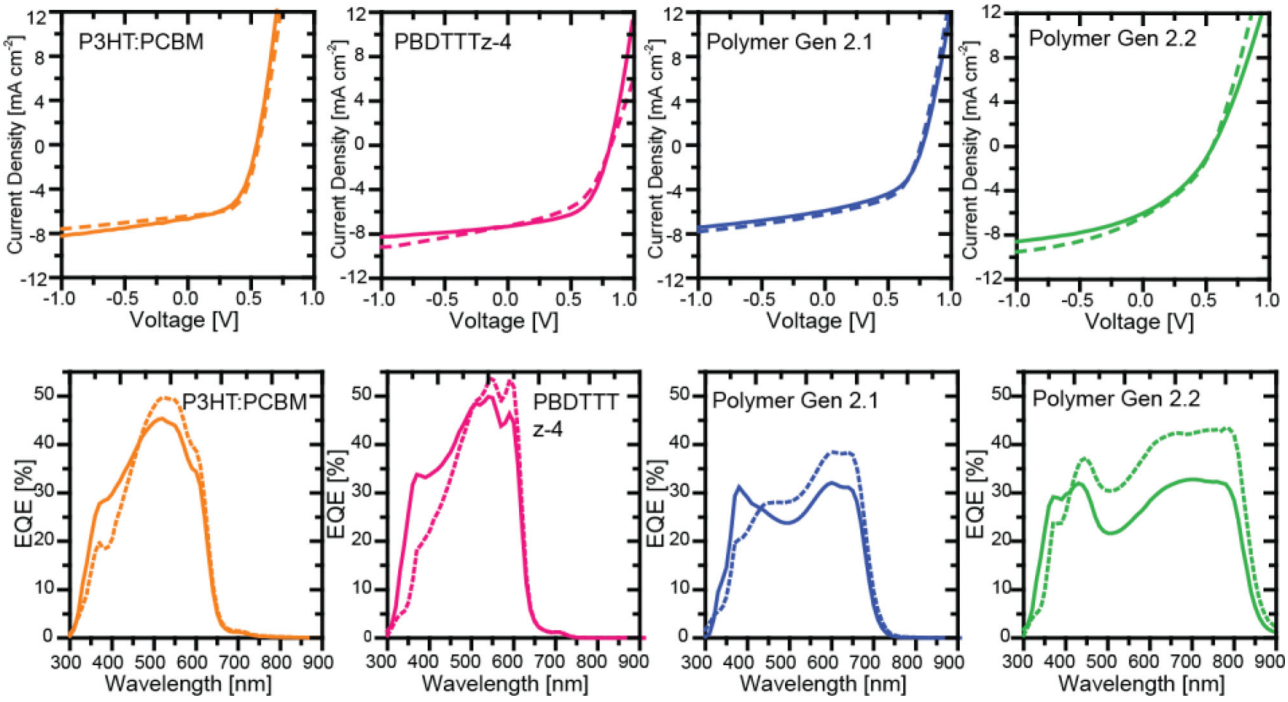


**Figure 6.** *IV* curves of the best single cell devices (top row) and EQE graphs of representative single cells (bottom row) based on AgNW electrode (dashed lines) and on Flextrode (solid lines).

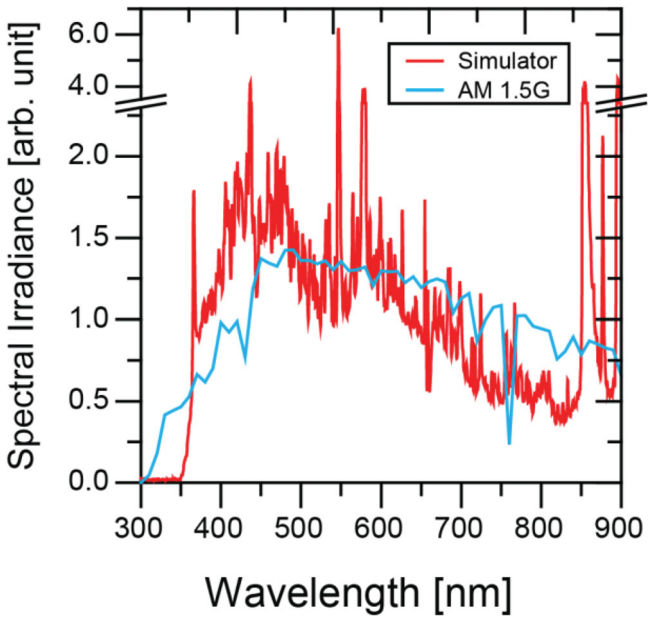


**Figure 7.** The spectrum of the solar simulator and AM1.5G spectrum.

absorption and the spectrum of the solar simulator which is not accounted for in tandem devices. The spectral mismatch in addition to the lower transmission of Flextrode further diminishes the current harvesting from the rear Polymer Generation 2.2 cell. Therefore, current in AgNW/ZnO-based tandem devices are significantly higher than in Flextrode based devices.

The efficiency of P3HT:PCBM/Polymer Generation 2.2:PCBM is higher than either of the individual single cells because of the most optimal current matching and highest enhancement in $V_{oc.}$ On the other hand, the efficiency of PBDTTTz-4:PCBM/Polymer Generation 2.2:PCBM tandem cells is lower in comparison to the best PBDTTTz-4:PCBM single cell that displays a PCE of >3% despite the similar absorption characteristics as P3HT:PCBM based tandem cells. This could be due to processing incompatibility as PBDTTTz-4:PCBM requires processing at 90 °C to achieve above 3% efficiency which is not maintained in the processing of tandem cells where all subsequent layers on top of the PDBTTTz-4:PCBM layer are best processed at 60–70 °C. Therefore, it is reasonable to believe that this polymer cannot perform as efficiently in a tandem structure in the processing regime employed in this study as it does in single cells.

The combination of Polymer Generation 2.1:PCBM/Polymer Generation 2.2:PCBM on AgNWs has significantly higher efficiency (2.17%) than on Flextrode (1.29%), however it is lower than the best single cell of Polymer Generation 2.1:PCBM (2.45%). This is because the tandem cell here suffers from overlap in the absorption spectrum which results in lower current in the current limiting rear cell. This effect is significantly more pronounced on Flextrode electrodes owing to the lower transmission for Polymer Generation 2.2 which in addition to the mismatch of the simulator emission spectrum with Polymer Generation 2.2 absorption characteristics further inhibits current generation in the rear cell and therefore undermines the PCE of the tandem devices appreciably more compared to AgNW based tandem devices.

Thus far, we discussed the tandem devices with respect to $J_{sc}$. The $V_{oc}$ of all tandem cells also suffers losses and it is not the sum of the $V_{oc}$ of the subcells. Several reasons explain this limitation. First, the lack of current matching as the devices are not optimized results in excessive current generation across the front subcell which could lead to compensation of the built-in field across the front subcell, ultimately lowering the net $V_{oc}$ for the tandem structure. It must be noted that the current in the rear subcell is limited because of lower illumination received by the rear cells which can be attributed to the overlap between its absorption spectrum and the absorption of the front-cell polymer (Figure 5) and the mismatch factor as explained in the previous segment. Furthermore, $V_{oc}$ could be limited by short circuits (shunts) owing to spikes in the substrates. Previously, we have employed a similar tandem cell, but on an extremely smooth opaque and reflective Ag-film substrate and have achieved complete recovery of $V_{oc}$.[40] Spikes in Ag grid in Flextrode devices have been shown earlier[41,46] to limit $V_{oc}$ in tandem devices. The loss in $V_{oc}$ in AgNW/ZnO based tandem devices was further investigated. The print edges of the ZnO layer are thinner than in the center which leads to exposed nanowires (**Figure 9**). Furthermore, the cracks in the ZnO layer could also contribute to shunting as these cracks are generally rather wide (200–500 nm) (Figure 7). Practically, this problem could be circumvented with the use of 400 nm thick front cells as this thickness showed no limitation in FF and current in single cells (Table 2). However, such a setup may not lead to the most optimal thickness and therefore a trade-off is required.

Finally, it must be stressed that the limitation in all the tandem cells investigated in this study is the performance of the rear cells based on Polymer Generation 2.2:PCBM. While this polymer has a band gap extremely suitable to be paired with other wider band gap polymers such as PDBTTTz-4:PCBM

**Table 3.** Mismatch factor calculated for all four polymers based on the spectrum of the solar simulator, AM1.5G spectrum, with respect to the absorption characteristics of the photoactive polymers.

| Polymer | Flextrode | | | AgNW | | |
|---|---|---|---|---|---|---|
| | Mismatch factor | $J_{sc}$ (EQE) | $J_{sc}$ (*IV*-mismatch corrected) | Mismatch factor | $J_{sc}$ (EQE) | $J_{sc}$ (*IV*-mismatch corrected) |
| P3HT | 1.09 | 5.93 | 6.91 (6.38 ± 0.41) | 1.09 | 6.20 | 6.65 (7.06 ± 0.62) |
| PBDTTTz-4 | 1.10 | 6.40 | 7.45 (7.52 ± 0.08) | 1.10 | 6.33 | 7.40 (6.98 ± 0.39) |
| Polymer Generation 2.1 | 1.03 | 5.42 | 6.51 (5.96 ± 0.34) | 1.01 | 6.24 | 6.97 (6.62 ± 0.53) |
| Polymer Generation 2.2 | 0.88 | 8.46 | 7.65 (7.81 ± 0.82) | 0.87 | 11.22 | 8.09 (7.91 ± 0.16) |

**Table 4.** *IV* parameters of best and average (minimum four devices) of roll-coated tandem solar cells on roll-to-roll processed AgNW/ZnO electrode and parallel devices on Flextrode. All measurements are under 1000 W $m^{-2}$ AM1.5G calibrated light source. Areas of all devices are accurately determined using LBIC imaging and are ≈0.8–1 $cm^2$.

| | Flextrode | | | | AgNW | | | |
|---|---|---|---|---|---|---|---|---|
| Polymer | $V_{oc}$ [V] | $J_{sc}$ [mA $cm^{-2}$] | FF [%] | PCE [%] | $V_{oc}$ [V] | $J_{sc}$ [mA $cm^{-2}$] | FF [%] | PCE [%] |
| P3HT (250 nm)/Polymer Generation 2.2 (350 nm) | 0.7 (0.73 ± 0.04) | 3.62 (2.36 ± 0.16) | 38.96 (38.25 ± 1.51) | 1.18 (1.11 ± 0.04) | 1.06 (1.02 ± 0.03) | 6.36 (5.75 ± 0.51) | 39.59 (38.10 ± 1.16) | 2.66 (2.51 ± 0.15) |
| PBDTTT (250 nm)/ Polymer Generation 2.2 (350 nm) | 1.00 (0.96 ± 0.09) | 5.86 (5.11 ± 0.41) | 36.67 (37.68 ± 1.66) | 2.28 (2.06 ± 0.12) | 1.06 (1.04 ± 0.08) | 6.93 (6.19 ± 0.43) | 34.99 (34.16 ± 2.70) | 2.53 (2.19 ± 0.14) |
| Polymer Generation 2.1 (250 nm)/Polymer Generation 2.2 (350 nm) | 1.04 (1.03 ± 0.03) | 3.26 (3.17 ± 0.11) | 37.96 (37.98 ± 0.54) | 1.29 (1.24 ± 0.06) | 1.00 (1.00 ± 0.04) | 6.06 (5.48 ± 0.46) | 36.64 (36.76 ± 00.87) | 2.17 (2.01 ± 0.11) |

and P3HT:PCBM, its inherent lower fill factor creates a bottleneck in the performance of all tandem devices. As such, the tandem devices in this study must be taken as an evaluation criterion for AgNW/ZnO and Flextrode. It must also be stressed that many of the alternatives of transparent conductors such as AgNW, Ag grids, Ag films, graphene, carbon nanotubes, etc., are topologically not similar to ITO. When used as a bottom electrode, the challenge with the use of alternative low-cost electrode is to avoid shunting due to the roughness and spikes in the substrate. Often this can be avoided with a larger thickness of intermediate layers between the counter electrodes. However, many high efficiency polymers cannot perform optimally when higher layer thicknesses are employed. As such, a tradeoff is always present. These complications, although seemingly trivial, results in the gap between the highest efficiency reported in literature which now reaches 11% and in devices that are realized through large-scale and commercially viable processing methods.

## 3. Conclusion

We have demonstrated rotary screen printing as a fast roll-to-roll processing method for printing of silver nanowire/zinc oxide electrode. The electrode is further employed in single and tandem cells and compared with our previously all-printed semi-transparent electrode known as Flextrode. Flextrode is very suitable for single cells based on wider band gap polymers such as P3HT:PCBM, whereas AgNW/ZnO electrodes are more suitable for lower band gap polymers in single cells. On the other hand, Flextrode is not optimal for tandem devices where its poor transmission in the longer wavelength region is prohibitive to achieving high efficiency tandem solar cells. In this case, AgNW/ZnO is significantly better than Flextrode. Although the efficiency of tandem cells is lower than single cells, there are reasons for this limitation including the challenge with the poorly performing low band gap polymer based rear cells and the spectral mismatch that cannot be accounted for in tandem devices. These issues can possibly be resolved in the future but will require further process and materials development. Nonetheless, this study confirms that rotary screen printing is a viable technique for printing of AgNW/ZnO electron accepting electrodes which can enable extremely fast processing of the electrode and that this electrode is a feasible ITO alternative particularly suited for tandem polymer solar cells.

## 4. Experimental Section

*Materials*: The substrate was 130 µm thick PET (Melinex ST506) purchased from Dupont-Teijin. The AgNW ink was purchased from Nanopyxis and had an average diameter of 35 ± 5 nm, average length 25 ± 5 µm, and a solid load of 1 wt%. ZnO nanoparticle solution was obtained from infinityPV in acetone with a concentration of 56 mg $mL^{-1}$. P3HT with a molecular weight of 40 kDa and a regioregularity of 96% was purchased from BASF (Sepiolid P200); PBDTTTz-4 were synthesized in-house following the procedures described elsewhere;[42] Polymer

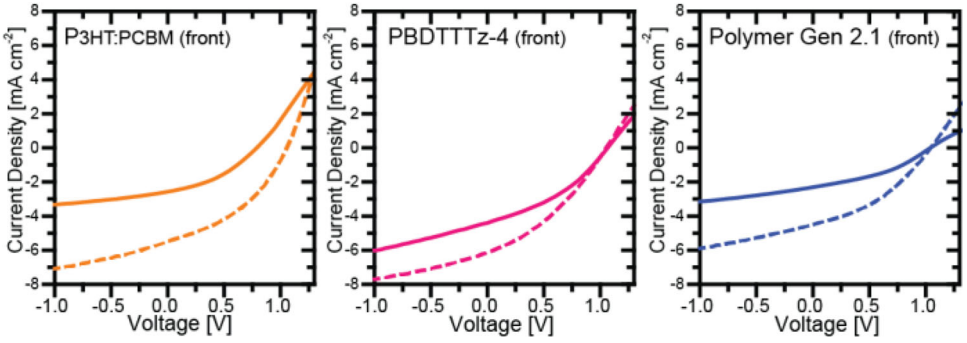


**Figure 8.** *IV* curves of the best tandem cells on AgNW/ZnO electrode (dashed lines) and on Flextrode (solid lines) with front subcell based on three different polymers indicated in the graphs. Polymer Gen 2.2 formed the back cell in all cases.

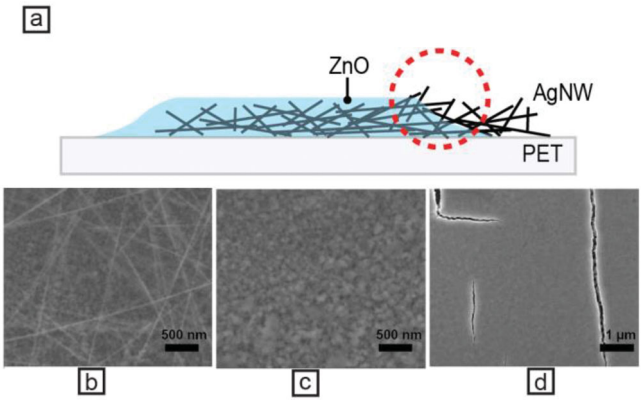


**Figure 9.** a) Schematic demonstration of cross section of AgNW/ZnO layers showing layer offsets carried out during printing. Red circle shows the shunt susceptible region. This edge corresponds to the SEM image shown in (b) where exposed AgNWs were observed due to lower thickness of ZnO at the edges. c) No AgNWs in the center of print stripe was observed. d) Cracks are seen in ZnO layer which could contribute to shunting.

Generation 2.2 and Polymer Generation 2.1 were received from Merck as previously described,[34] [60] PCBM with a purity of 99% was purchased from Merck. Two different PEDOT:PSS formulations from Heraeus were used in this study—Clevios F-010 and Clevios P VP AL 4083. Thermally curable Ag (PV410) paste was purchased from DuPont. All devices were encapsulated between two glass slides which were fixed to each cell by using a UV curable adhesive from DELO (DELO–Katibobond LP 655).

*Device Processing*: AgNW and ZnO layers were roll-to-roll fabricated in stripes on PET of 100 m length and a web width of 305 mm using two discrete roll-to-roll steps with only one printing technique. The nanowire ink was coated as purchased using rotary screen printing at a speed of 10–20 m $min^{-1}$ which means the drying time through our 4 m long oven at 140 °C was <30 s while ZnO was coated at a speed of 20 m $min^{-1}$ which allowed a drying time of merely 12 s. The remaining stacks were fabricated on a mini roll coater using 1 m of this substrate sliced from the R2R fabricated AgNW/ZnO roll. All except the top Ag grid was slot-die coated on a mini roll coater. All photoactive layers were slot die coated at 70 °C except for PBDPTTTz-4 which requires 90 °C. The web speed and flow were optimized to achieve the required thickness. The active ink composition were as follows: P3HT:PCBM was mixed in 1:1 wt/wt ratio with a concentration of 40 mg $mL^{-1}$ of solvent comprising of chlorobenzene mixed with 3 vol% 1-chloronaphthalene as an additive; PBDTTTz-4:PCBM was mixed in 1:1.5 wt/wt ratio with a concentration of 30 mg $mL^{-1}$ in a solvent mixture comprising of 1,2-dicholorobenzene mixed with 3 vol% 1-chloronaphthalene. Polymer Generation 2.1:PCBM was mixed in 1:1.5 wt/wt with a solid load of 44 mg $mL^{-1}$ in chloroform; and Polymer Generation 2.2:PCBM mixed in 1:2.5 wt/wt ratio with solid concentration of 37.50 mg $mL^{-1}$ was dissolved in o-xylene mixed with 10 vol% tetralin. The recombination layer comprised of three layers as previously described.[40,41] Briefly, the first PEDOT:PSS layer was based on Clevios F-010 diluted with isopropanol (IPA) in 1:4 vol/vol which was used as a wetting agent/compatibilizer. This layer was slot-die coated at a speed of 1.25 m $min^{-1}$ and flow rate of 0.10 mL $min^{-1}$. The second PEDOT:PSS layer comprised of Clevios P VP AL 4083 diluted with IPA in 1:1 v/v which was slot-die coated on top of the compatibilizer layer at the same speed and a flow rate of 0.30 mL $min^{-1}$. Finally, the recombination layer was completed by slot-die coating ZnO at a speed of 2 m $min^{-1}$ and a flow rate of 0.08 mL $min^{-1}$ resulting in a dry layer thickness of 40 nm. All three layers in the recombination were coated at 60 °C. The PEDOT:PSS top electrode comprised of three layers as described elsewhere.[40,41] Finally, the Ag grid was flexo printed. All devices were annealed at 110 °C for 5 min postfabrication. Individual cells were cut from each stripe, and randomly characterized before and after encapsulation. Devices were encapsulated between two microscopy slides with the use of DELO adhesive which required UV exposure accomplished under the solar simulator itself. All data presented are of encapsulated devices.

*Instrumentation*: *IV* characteristics were measured using a Keithley 2400 source meter and illumination was provided KHS SolarConstant 575 solar simulator (Steuernagel Lichtteknik) which was calibrated with a reference photodiode to 100 mW $cm^{-2}$ AM1.5G. Transmittance was measured with a UV–vis spectrophotometer (Shimadzu UV-1700). A Jandel RM3 4-point probe station was used to measure the sheet resistance. SEM images were acquired using a field-emission gun SEM (Zeiss Supra 35) operated at electron gun acceleration voltage of 5 kV, pressure of $<8 \times 10^{-6}$ mbar, working distance of 5 mm, and using a lateral secondary electron detector and an InLens detector. Samples were precoated with 5–10 nm of carbon using sputter coater. An in-house built laser beam induced imaging (LBIC) instrument was employed in accurately determining the active area of all devices.[32]

## Acknowledgements

Financial support to carry out this work was received from the Danish National Research Foundation, the Villum Foundation's Young Investigator Programme (second round, Project: Materials for Energy Production). Partial financial support was also received from the European Commission as part of the Framework 7 (Grant No. 288565), DFG in the frame of SPP 1355 Elementary processes in organic photovoltaics; the Danish Ministry of Science, Innovation and Higher Education under a Sapere Aude Top Scientist grant (No. DFF-1335-00037A) and an Elite Scientist grant (No. 11-116028).

Received: May 7, 2015
Published online: June 18, 2015

[1] N. Espinosa, R. García-Valverde, A. Urbina, F. C. Krebs, *Solar Energy Mater. Solar Cells* **2011**, *95*, 1293.
[2] C. J. Emmott, A. Urbina, J. Nelson, *Solar Energy Mater. Solar Cells* **2012**, *97*, 14.
[3] J. You, L. Dou, K. Yoshimura, T. Kato, K. Ohya, T. Moriarty, K. Emery, C. Chen, J. Gao, G. Li, *Nat. Commun.* **2013**, *4*, 1446.
[4] C. Chen, W. Chang, K. Yoshimura, K. Ohya, J. You, J. Gao, Z. Hong, Y. Yang, *Adv. Mater.* **2014**, *26*, 5670.
[5] D. Angmo, F. C. Krebs, *J. Appl. Polym. Sci.* **2013**, *129*, 1.
[6] K. Ellmer, *Nat. Photonics* **2012**, *6*, 808.
[7] D. Langley, G. Giusti, C. Mayousse, C. Celle, D. Bellet, J. Simonato, *Nanotechnology* **2013**, *24*, 452001.
[8] D. A. Dinh, K. N. Hui, K. S. Hui, J. Singh, P. Kumar, W. Zhou, *Rev. Adv. Sci. Eng.* **2013**, *2*, 324.
[9] J. Krantz, T. Stubhan, M. Richter, S. Spallek, I. Litzov, G. J. Matt, E. Spiecker, C. J. Brabec, *Adv. Funct. Mater.* **2013**, *23*, 1711.
[10] Y. C. Lu, K. S. Chou, *Nanotechnology* **2010**, *21*, 215707.
[11] T. Kim, A. Canlier, G. H. Kim, J. Choi, M. Park, S. M. Han, *ACS Appl. Mater. Interfaces* **2013**, *5*, 788.
[12] F. Guo, X. Zhu, K. Forberich, J. Krantz, T. Stubhan, M. Salinas, M. Halik, S. Spallek, B. Butz, E. Spiecker, T. Ameri, N. Li, P. Kubis, D. M. Guldi, G. J. Matt, C. J. Brabec, *Adv. Energy Mater.* **2013**, *3*, 1062.
[13] J. Lee, S. T. Connor, Y. Cui, P. Peumans, *Nano Lett.* **2008**, *8*, 689.
[14] J. Lee, S. T. Connor, Y. Cui, P. Peumans, *Nano Lett.* **2010**, *10*, 1276.
[15] B. E. Hardin, W. Gaynor, I.-. Ding, S. Rim, P. Peumans, M. D. McGehee, *Org. Electron.* **2011**, *12*, 875.
[16] C. Chung, T. Song, B. Bob, R. Zhu, Y. Yang, *Nano Res.* **2012**, *5*, 805.
[17] D. Leem, A. Edwards, M. Faist, J. Nelson, D. D. C. Bradley, J. C. de Mello, *Adv. Mater.* **2011**, *23*, 4371.

[18] M. Song, J. H. Park, C. S. Kim, D. Kim, Y. Kang, S. Jin, W. Jin, J. Kang, *Nano Res.* **2014**, *7*, 1370.
[19] L. Hu, H. S. Kim, J. Lee, P. Peumans, Y. Cui, *ACS Nano* **2010**, *4*, 2955.
[20] L. Hu, H. Wu, Y. Cui, *MRS Bull.* **2011**, *36*, 760.
[21] C. Liu, X. Yu, *Nano Res. Lett.* **2011**, *6*, 75.
[22] S. De, T. M. Higgins, P. E. Lyons, E. M. Doherty, P. N. Nirmalraj, W. J. Blau, J. J. Boland, J. N. Coleman, *ACS Nano* **2009**, *3*, 1767.
[23] L. Yang, T. Zhang, H. Zhou, S. C. Price, B. J. Wiley, W. You, *ACS Appl. Mater. Interfaces* **2011**, *3*, 4075.
[24] T. Tokuno, M. Nogi, M. Karakawa, J. Jiu, T. T. Nge, Y. Aso, K. Suganuma, *Nano Res.* **2011**, *4*, 1215.
[25] E. C. Garnett, W. Cai, J. J. Cha, F. Mahmood, S. T. Connor, M. G. Christoforo, Y. Cui, M. D. McGehee, M. L. Brongersma, *Nat. Mater.* **2012**, *11*, 241.
[26] C. Celle, C. Mayousse, E. Moreau, H. Basti, A. Carella, J. Simonato, *Nano Res.* **2012**, *5*, 427.
[27] J. Ajuria, I. Ugarte, W. Cambarau, I. Etxebarria, R. Tena-Zaera, R. Pacios, *Solar Energy Mater. Solar Cells* **2012**, *102*, 148.
[28] W. Gaynor, J. Lee, P. Peumans, *ACS Nano* **2010**, *4*, 30.
[29] W. Gaynor, G. F. Burkhard, M. D. McGehee, P. Peumans, *Adv. Mater.* **2011**, *23*, 2905.
[30] F. C. Krebs, M. Hösel, M. Corazza, B. Roth, M. V. Madsen, S. A. Gevorgyan, R. R. Søndergaard, D. Karg, M. Jørgensen, *Energy Technol.* **2013**, *1*, 378.
[31] InfinityPV, http://infinitypv.com/infinitypro/flextrode (Accessed: February 2015) and http://plasticphotovoltaics.org/flextrode.html (accessed: February 2015).
[32] D. Angmo, S. A. Gevorgyan, T. T. Larsen-Olsen, R. R. Søndergaard, M. Hösel, M. Jørgensen, R. Gupta, G. U. Kulkarni, F. C. Krebs, *Org. Electron.* **2013**, *14*, 984.
[33] M. Hösel, R. R. Søndergaard, M. Jørgensen, F. C. Krebs, *Energy Technol.* **2013**, *1*, 102.
[34] T. R. Andersen, H. F. Dam, M. Hösel, M. Helgesen, J. E. Carlé, T. T. Larsen-Olsen, S. A. Gevorgyan, J. W. Andreasen, J. Adams, N. Li, F. Machui, G. D. Spyropoulos, T. Ameri, N. Lemaître, M. Legros, A. Scheel, D. Gaiser, K. Kreul, S. Berny, O. R. Lozman, S. Nordman, M. Välimäki, M. Vilkman, R. R. Søndergaard, M. Jørgensen, C. J. Brabec, F. C. Krebs, *Energy Environ. Sci.* **2014**, *7*, 2925.
[35] M. Hösel, D. Angmo, R. R. Søndergaard, G. A. dos Reis Benatto, J. E. Carlé, M. Jørgensen, F. C. Krebs, *Adv. Sci.* **2015**, *1*, 1400002.
[36] F. C. Krebs, *Sol. Energy Mater. Sol. Cells* **2009**, *93*, 394.
[37] R. R. Søndergaard, M. Hösel, F. C. Krebs, *J. Polym. Sci., Part B: Polym. Phys.* **2013**, *51*, 16.
[38] A. Kim, Y. Won, K. Woo, C. Kim, J. Moon, *ACS Nano* **2013**, *7*, 1081.
[39] F. S. F. Morgenstern, D. Kabra, S. Massip, T. J. K. Brenner, P. E. Lyons, J. N. Coleman, R. H. Friend, *Appl. Phys. Lett.* **2011**, *99*, 183307.
[40] D. Angmo, H. F. Dam, T. R. Andersen, N. K. Zawacka, M. V. Madsen, J. Stubager, F. Livi, R. Gupta, M. Helgesen, J. E. Carlé, T. T. Larsen-Olsen, G. U. Kulkarni, E. Bundgaard, F. C. Krebs, *Energy Technol.* **2014**, *2*, 651.
[41] T. R. Andersen, H. F. Dam, B. Andreasen, M. Hösel, M. V. Madsen, S. A. Gevorgyan, R. R. Søndergaard, M. Jørgensen, F. C. Krebs, *Sol. Energy Mater. Sol. Cells* **2014**, *120*, 735.
[42] J. E. Carlé, M. Helgesen, M. V. Madsen, E. Bundgaard, F. C. Krebs, *J. Mater. Chem. C* **2014**, *2*, 1290.
[43] S. R. Cowan, A. Roy, A. J. Heeger, *Phys. Rev. B* **2010**, *82*, 245207.
[44] R. Mauer, I. A. Howard, F. Laquai, *J. Phys. Chem. Lett.* **2010**, *1*, 3500.
[45] J. Y. Kim, K. Lee, N. E. Coates, D. Moses, T. Q. Nguyen, M. Dante, A. J. Heeger, *Science* **2007**, *317*, 222.
[46] T. R. Andersen, H. F. Dam, B. Burkhart, D. Angmo, M. Corazza, B. C. Thompson, F. C. Krebs, *J. Mater. Chem. C* **2014**, *2*, 9412.